# Cyclotron Resonance in Copper*

A. F. KIP, D. N. LANGENBERG,† AND T. W. MOORE
*Department of Physics, University of California, Berkeley, California*
(Received June 6, 1961)

Extensive cyclotron resonance experiments in copper at 24 kMc/sec are described. The results are consistent with the Azbel'-Kaner theory of cyclotron resonance in metals and with the known Fermi surface geometry. "Stationary" orbits (orbits having extremal effective mass and vanishing average velocity in the magnetic field direction) are found to dominate the cyclotron resonance signals in copper. The effective mass anisotropy of various classes of stationary orbits is reported. The effects of tipping the magnetic field slightly out of the plane of the sample surface and of the direction of the rf currents with respect to the magnetic field are described.

## I. INTRODUCTION

THE success of cyclotron resonance experiments in determining the band structure of semiconductors[1,2] suggested the extension of this technique to metals. Azbel' and Kaner[3] were the first to present a solution of the appropriate transport problem and indicated how cyclotron resonance might be observed in metals. Azbel'-Kaner resonances have subsequently been observed in a number of metals. We report here the results of extensive cyclotron resonance experiments on a single crystal of copper.

We consider here only the Azbel'-Kaner type experiment in which the static magnetic field is essentially parallel to a plane surface of a single-crystal metal sample. Cyclotron resonance in metals is similar to the more familiar (bulk) cyclotron resonance in semiconductors in that it depends on the resonant response to microwave fields at magnetic fields $H_c$ such that the cyclotron frequency of the orbiting carriers ($\omega_c = eH/m^*c$) equals the rf frequency $\omega$, where $m^*$ is the cyclotron effective mass. Thus both experiments require samples of sufficient purity and uniform crystal structure so that $\omega\tau > 1$, where $\tau$ is the electron relaxation time, and are performed at temperatures (typically in the liquid helium range) such that $\tau$ is impurity or defect limited.

However, in contrast to the bulk experiment which is performed at carrier concentrations for which the skin depth is very much greater than the diameter of carrier orbits and the sample dimensions, the experiment in metals is performed under anomalous skin effect conditions (as a consequence of the high carrier density and the necessarily long relaxation times) where the penetration depth of rf fields is typically two orders of magnitude smaller than the radius of carrier orbits.

This brings about several important differences between the two experiments. During each cyclotron period an electron interacts with the rf field for a time short compared with either the cyclotron period or the rf period. Resonance will occur if the electron makes each rapid traversal of the penetration depth at the same point in an rf period, i.e., if $\omega_c = \omega/n$ where $n$ is a nonzero integer. Thus in metals, resonances observed at constant $\omega$ will appear at a field $H_c = m^*c\omega/e$ and also at fields $H_c/n$. The resonances at $H_c/n$ are called subharmonic resonances because the cyclotron frequency at each of these resonances is a subharmonic of the constant rf frequency. It should be emphasized that the subharmonic resonances occur even for spherical energy surfaces in contrast to the semiconductor case in which weak harmonic resonances are sometimes observed for warped, nonquadratic energy surfaces.[4] The origin of the subharmonics in the two cases is quite different.

Since the rf fields interact with the carriers over only a very small part of their orbits, it is impossible to detect the sense of the cyclotron rotation (i.e., the sign of the charge-to-mass ratio) as can be done in semiconductors or in metals with the static magnetic field perpendicular to the sample surface[5] by using circularly polarized rf fields.

At resonance the rf power absorption is a minimum in metals but a maximum in semiconductors. This does not reflect any fundamental difference in the resonance phenomena in the two cases but only a difference in the experimental conditions imposed by the high conductivity of metals on the one hand and the low conductivity of semiconductors on the other. In each case the conductivity at resonance is a maximum.[6]

A typical cyclotron resonance absorption derivative signal in copper is shown in the top panel of Fig. 1, in which the second through twelfth subharmonics are clearly visible; the bottom panel shows the signal predicted for a free electron metal by Azbel' and Kaner for $\omega\tau = 10$.

The cyclotron effective mass may be determined with the precision of resonance methods either from $H_c$ ($m^* = eH_c/\omega c$) or from the periodicity in $1/H$, $\Delta(1/H)$, of the subharmonic resonances [$m^* = e/\omega c\Delta(1/H)$]. In

* This work has been supported in part by the Office of Naval Research and by the Air Force Office of Scientific Research.
† Present address: Department of Physics, University of Pennsylvania, Philadelphia, Pennsylvania.
[1] G. Dresselhaus, A. F. Kip, and C. Kittel, Phys. Rev. **98**, 368 (1955).
[2] R. N. Dexter, H. J. Zeiger, and B. Lax, Phys. Rev. **104**, 637 (1956).
[3] M. Ya. Azbel' and E. A. Kaner, J. Phys. Chem. Solids **6**, 113 (1958).
[4] B. Lax, Phys. Rev. Letters **4**, 511 (1960).
[5] J. K. Galt, W. A. Yager, F. R. Merritt, B. B. Cetlin, and A. D. Brailsford, Phys. Rev. **114**, 1396 (1959).
[6] R. G. Chambers, Phil. Mag. **1**, 459 (1956).

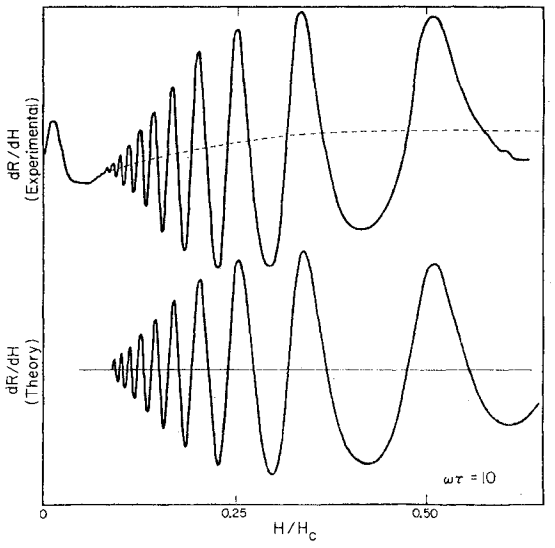


FIG. 1. Comparison between a typical cyclotron resonance absorption derivative trace and the theoretical prediction of Azbel' and Kaner for $\omega\tau=10$.

addition, the existence of various types of orbits can yield much information about the shape of the Fermi surface, although this is well known in the present experiments. Also, as we shall show below, the electron relaxation time may be determined from the relative magnitudes of the subharmonic resonances, and some information about the details of the effective-mass distribution may be inferred from the resonance line shape.

Shockley[7] has shown that the cyclotron mass of an orbit is related to the energy band structure by the relation

$$m^*=(\hbar^2/2\pi)(\partial A/\partial E), \tag{1}$$

where $A$ is the cross sectional area of the orbit in wave-vector space and $E$ is the electron energy. Thus a knowledge of the shape of the Fermi surface and of the anisotropy of the effective mass enables one to reconstruct $\Delta_k E(\mathbf{k})$ over the Fermi surface, and the density of states and the Fermi velocities may be computed.

Azbel'-Kaner experiments have been performed on a number of pure metals. The first experiments to give an indication of success were performed by Fawcett[8] in 1956 on tin and copper. No subharmonics were observed in these experiments. Experiments on tin by Kip, Langenberg, Rosenblum, and Wagoner[9] showed as many as 13 subharmonics and also showed patterns of two or more sets of subharmonics, indicating that several different cyclotron masses were being observed for a given crystal orientation. More recently, Khaikin[10] has also observed many subharmonics in tin. Bezuglyi and Galkin[11,12] observed resonance in tin and lead, but saw no subharmonics, and Aubrey[13] has observed subharmonics in lead, using a cylindrical sample. Aluminum has been studied by Langenberg and Moore[14] and by Fawcett.[15] Cyclotron resonance in zinc has been observed by Galt, Merritt, Yager, and Dail[16] and in antimony by Dexter and Datars.[17] Bismuth has been studied by Aubrey and Chambers[18] and by Galt *et al.*[5,19] Preliminary results of the present work in copper have been reported previously.[20]

This is the first cyclotron resonance study in metals in which (i) the mass anisotropy (that is, the dependence of the mass on the orientation of the magnetic field with respect to the crystal axes) has been determined, (ii) the resonating orbits have been identified on the Fermi surface, and (iii) the dependence of the effect on the direction of the rf currents with respect to the crystal axes (rf polarization) and on the angle between the magnetic field and the sample surface (field tipping) has been investigated in detail. These last two effects are an almost indispensable aid in orbit selection and identification, especially in a metal like copper in which many types of orbits are possible as a consequence of the zone boundary contacts (see, for example, Lifshitz and Peschanskii[21]).

## II. THEORY

As a consequence of the condition $\omega\tau>1$, cyclotron resonance experiments in metals are performed under anomalous skin effect conditions, where the mean free path $l$ is greater than the classically computed skin depth $\delta=(2\pi\omega\sigma/c^2)^{-\frac{1}{3}}$. Thus Ohm's law, which is a point relation between currents and fields, fails, and a computation of the surface impedance requires the use of a more general transport theory with the nature of the carrier scattering at the surface imposed as a boundary condition.

Such treatment have been made by Pippard[22,23] and

[7] W. Shockley, Phys. Rev. **79**, 191 (1950).
[8] E. Fawcett, Phys. Rev. **103**, 1582 (1956).
[9] A. F. Kip, D. N. Langenberg, B. Rosenblum, and G. Wagoner, Phys. Rev. **108**, 494 (1957).
[10] M. S. Khaikin, Soviet Phys.—JETP **10**, 1044 (1960).
[11] P. A. Bezuglyi and A. A. Galkin, Soviet Phys.—JETP **7**, 163 (1958).
[12] P. A. Bezuglyi and A. A. Galkin, Soviet Phys.—JETP **7**, 164 (1958).
[13] J. E. Aubrey, Phil. Mag. **5**, 1001 (1960).
[14] D. N. Langenberg and T. W. Moore, Phys. Rev. Letters **3**, 137 (1959).
[15] E. Fawcett, Phys. Rev. Letters **3**, 139 (1959).
[16] J. K. Galt, E. R. Merritt, W. A. Yager, and H. W. Dail, Jr., Phys. Rev. Letters **2**, 292 (1959).
[17] R. N. Dexter and W. R. Datars, Paper presented at International Conference on Electronic Properties of Metals at Low Temperatures, Geneva, New York, 1958 (unpublished); W. R. Datars and R. N. Dexter, Phys. Rev. **124**, 75 (1961).
[18] J. E. Aubrey and R. G. Chambers, J. Phys. Chem. Solids **3**, 128 (1957).
[19] J. K. Galt, W. A. Yager, F. R. Merritt, B. B. Cetlin, and H. W. Dail, Jr., Phys. Rev. **100**, 748 (1955).
[20] D. N. Langenberg and T. W. Moore, Phys. Rev. Letters **3**, 328 (1959).
[21] I. M. Lifshitz and V. G. Peschanskii, Soviet Phys.—JETP **11**, 137 (1960).
[22] A. B. Pippard, *Advances in Electronics and Electron Physics*, edited by L. Marton (Academic Press, Inc., New York, 1954), Vol. 6.
[23] A. B. Pippard, *Reports on Progress in Physics* (The Physical Society, London, 1960), Vol. 23.

Reuter and Sondheimer[24] for the anomalous skin effect and by Pippard,[23] Heine,[25] Azbel' and Kaner,[3] Rodriguez,[26] and Mattis and Dresselhaus[27] for cyclotron resonance. We shall only quote the results of these exact treatments here, and discuss some of the qualitative aspects which affect cyclotron resonance.

Under anomalous skin-effect conditions in the absence of a magnetic field we can see immediately that electrons leaving the surface at angles such that they do not undergo a collision before they have penetrated many skin depths into the metal cannot acquire any net momentum parallel to the surface. If they did, currents and thus fields would exist many skin depths below the surface, contradicting the assumption of the existence of a skin depth. Exact treatments show that rf fields do not penetrate metals exponentially under these conditions, but exist in space and time in such a way that electrons traveling away from the surface acquire no net transverse momentum. Nevertheless, the fields are confined within a region close to the surface of the same order of magnitude as the classical skin depth. These observations form the basis of Pippard's[22] "ineffectiveness concept," which assumes that only those carriers whose paths make an angle less than $\beta\delta/l$ with the surface are effective in transport processes, where $\beta$ is expected to be of the order of unity. Using this simple concept, Pippard derived an expression for the complex surface impedance $Z$, which is essentially the same as the result of a more rigorous treatment, but with $\beta$ about 10 for the best fit.

If we assume (i) diffuse reflection of electrons at the surface, and (ii) that the surface impedance tensor $Z$ may be reduced to principal axes, the results of exact treatment are given by

$$Z_{xx,yy} \propto e^{i\pi/3}\left(\frac{\omega^2 l}{\sigma}\right)^{\frac{1}{3}}\left[\Sigma\int_0^{2\pi}\frac{\cos^2\varphi,\sin^2\varphi}{K(\varphi)}d\varphi\right]^{-\frac{1}{3}}. \quad (2)$$

The angle $\varphi$ is measured from the $x$ axis and $K(\varphi)$ is the Gaussian curvature of the Fermi surface, both measured in the plane $v_z=0$ as shown in Fig. 2. The sum is over disconnected parts of the Fermi surface. The dependence on $K(\varphi)$ may be understood quite simply in terms of the ineffectiveness concept: The number of electrons whose velocities lie within an angle $\beta\delta/l$ of the sample surface is roughly proportional to the area of the Fermi surface whose normals lie within this angle, since the velocity [proportional to $\Delta_k(k)$] is normal to the surface. This area is inversely proportional to $K(\varphi)$. It was from measurements of this curvature that Pippard[28] deduced his model of the Fermi surface of copper, which we shall use in analyzing the cyclotron resonance results. Note that the frequency dependence of the anomalous surface impedance is proportional to $\omega^{\frac{2}{3}}$ rather than to $\omega^{\frac{1}{2}}$ as in the classical case, that the phase factor is $e^{i\pi/3}$ instead of $e^{i\pi/2}$, and that $Z$ is independent of $\sigma$, since $l/\sigma$ is a constant of the metal.

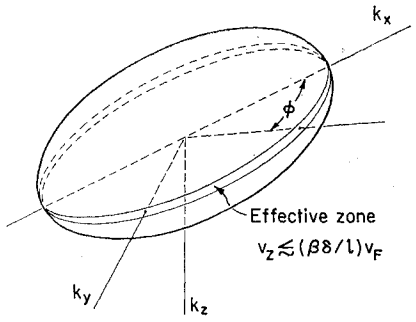


FIG. 2. A Fermi surface in $\mathbf{k}$ space, showing the effective zone for the anomalous skin effect. The sample surface is the $x$-$y$ plane. $\phi$ is the angle between the $x$ axis and the perpendicular to the Fermi surface.

Now consider the surface impedance under anomalous skin effect conditions in the presence of a magnetic field parallel to the surface of the metal. Before examining the results of exact treatment, let us consider a few qualitative aspects of the problem.

At available microwave frequencies, the condition $\omega\tau>1$ for cyclotron resonance is much more stringent than the requirement $l>\delta$ for the anomalous skin effect (for $\omega\approx 10^{11}$, $\delta$ is typically of the order of $10^{-5}$ cm, while the circumference of electron orbits at resonance for $m^*=m_e$ is approximately $10^{-3}$ cm).

The electron trajectories are governed by the Lorentz equation

$$\hbar d\mathbf{k}/dt=(e/c)[(1/\hbar)\Delta_k E(\mathbf{k})\times\mathbf{H}],$$

if we neglect the weak perturbing forces of the rf fields, while the electron energy is not changed by the presence of the magnetic field. Thus the component of wave vector parallel to $\mathbf{H}$, $k_H$, is a constant of the motion and may be used to label the orbit. The electron orbit cross sections in real space have the same shape as the Fermi surface cross sections of constant $k_H$, scaled by $c\hbar/eH$ and rotated by $\pi/2$ about $\mathbf{H}$.

The average velocity of an electron is

$$\mathbf{v}_D=\frac{1}{\hbar T_c}\int_0^{T_c}\Delta_k E(\mathbf{k})dt,$$

where $T_c$ is the cyclotron period, and $\mathbf{v}_D$ is parallel to $\mathbf{H}$. Harrison[29] has shown that a necessary and sufficient condition that $\mathbf{v}_D$ vanish is that $\partial A/\partial k_H=0$, where $A$ is the orbit cross-sectional area in wave-vector space. Since $\mathbf{v}_D$ is general is not zero, the electron trajectories are helices about $\mathbf{H}$. Unless $\mathbf{H}$ is aligned parallel to the surface within an angle $\alpha\approx\delta/v_D\tau$, the electrons will spiral out of the skin depth before suffering a collision,

[24] G. E. H. Reuter and E. H. Sondheimer, Proc. Roy. Soc. (London) **A195**, 336 (1948).
[25] V. Heine, Phys. Rev. **107**, 431 (1957).
[26] S. Rodriguez, Phys. Rev. **112**, 1616 (1958).
[27] D. C. Mattis and G. Dresselhaus, Phys. Rev. **111**, 403 (1958).
[28] A. B. Pippard, Phil. Trans. Roy. Soc. London **A250**, 325 (1957).
[29] W. A. Harrison, Phys. Rev. **118**, 1182 (1960).

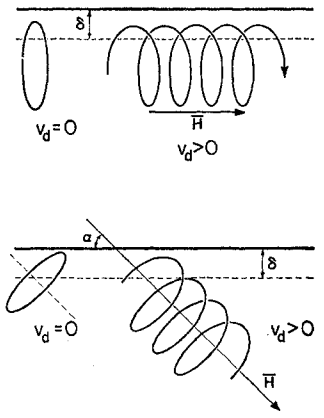


FIG. 3. Carrier orbits for **H** in the plane of the sample (top panel) and for **H** tipped at an angle $\alpha$ with respect to the sample surface (bottom panel).

and the size of the resonance signal will thus be reduced. This situation is illustrated in Fig. 3. Since $v_D \lesssim v_F \approx 10^8$ cm sec$^{-1}$, where $v_F$ is the Fermi velocity, and $\tau \approx 10^{-10}$ sec for $\omega\tau = 10$ at $\omega \approx 10^{11}$, $\alpha$ may be as small as $10^{-3}$, imposing severe experimental requirements both on field alignment and surface smoothness. Of course those orbits for which $v_D = 0$ will not be affected by small angle tipping. In addition, as we shall see below, there is also a mechanism which may actually tend to enhance the resonance when the field is tipped, thus easing the requirement for field alignment in some cases.

Shockley[30] has shown that in the case of quadratic (spherical or ellipsoidal) energy surfaces the cyclotron frequency $\omega_c(k_H)$, and thus the cyclotron mass $m^*(k_H)$, is the same for all orbits, independent of $k_H$. Such is the case in the conduction bands of silicon and germanium, and also perhaps in some zones of semimetals such as bismuth. However, in most real metals $m^*$ is a rather strong function of $k_H$, and we might expect that this "mass spread" would tend to dephase the resonance and thus wash it out, or at least drastically affect its nature. A simple consideration of the number of carriers having cyclotron masses $m^*(k_H) \pm \Delta m^*$ indicates that the resonance should be dominated by orbits $k_H{}^0 \pm \Delta k_H$ where $m^*(k_H{}^0)$ is extremal with respect to $k_H$ and

$$\Delta m^* \approx \tfrac{1}{2}[d^2m^*(k_H{}^0)/d^2k_H](\Delta k_H)^2.$$

The conditions that $m^*(k_H)$ be extremal ($\partial m^*/\partial k_H = 0$) and that $v_D$ vanish ($\partial A/\partial k_H = 0$) are often simultaneously required by symmetry considerations (for example, $k_H = 0$ orbits for a simple, closed Fermi surface). We shall call such orbits *stationary orbits*, after Ziman[31]; it will turn out that they play a dominant role in cyclotron resonance in copper.

If the mass spread is large, field tipping may actually enhance the resonance since those electrons which do not spiral out of the skin depth may have a more uniform mass distribution. Thus there are two competing mechanisms affecting the size of the resonance when the field is tipped; fewer electrons participate in the resonance, tending to weaken the signal, but there is less mass spread, tending to strengthen the signal. Both of these effects have been observed experimentally and have also been verified by exact calculation for absorption derivative signals.

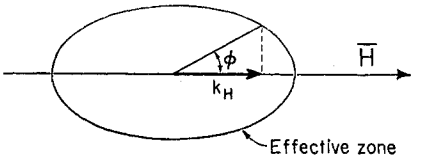


FIG. 5. Relationship between $k_H$ and $\varphi$ in Eq. (3). **H** is parallel to the $x$ axis. (*Note added in proof:* $\phi$ should be drawn between the field direction and the normal to the Fermi surface.)

Next consider the effect of the direction of linear rf currents with respect to the static magnetic field, that is, the effect of rf polarization. The contribution to the rf currents and hence to the losses by any orbit will be proportional to $\Delta_k E_k(k_H) \cdot \mathbf{j}_{rf}$ evaluated at the point on the orbit in $k$ space corresponding to the transit of the real space orbit through the skin depth. As illustrated in Fig. 4 those carriers which lie on parts of the Fermi surface normal to the current direction in the effective zone will dominate conduction processes. Thus, in Fig. 4(a), with the rf currents perpendicular to the static magnetic field, the region about the stationary orbit $k_H = 0$ will contribute most of the current, and the resonance will be "twice favored" in that the mass is extremal and the drift velocity is zero. In Fig. 4(b), on the other hand, electrons with large values of $k_H$ will dominate, and these orbits are not stationary; they will have drift velocities $v_D \lesssim v_F$, and $dm^*(k_H)/dk_H$ may also be large, so that the resonance may be relatively weak. The stationary orbits $k_H = 0$ will not contribute to the current in this case. Even if there is no mass spread, practical considerations of field alignment will make the resonance difficult to detect in this case, and place severe restrictions on the flatness of the surface. Thus, sensi-

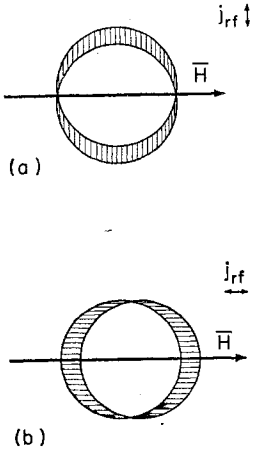


FIG. 4. Displacements of the Fermi surface for $\mathbf{j}_{rf}$ perpendicular and parallel to **H**.

[30] W. Shockley, Phys. Rev. **90**, 491 (1953).

[31] J. M. Ziman (private communication).

tivity to field tipping will be much greater for parallel polarization, and perpendicular polarization will usually be the favorable mode.

The most detailed and rigorous theoretical analysis of cyclotron resonance in metals has been made by Azbel' and Kaner.[3] They formulate the problem in terms of the Boltzmann transport equation and Maxwell's equations, imposing diffuse reflection of carriers at the surface as a boundary condition. If some small, almost constant magnetoresistance terms are neglected, their results in the resonance region are given by

$$Z_{xx,yy}(H) \propto \left[\Sigma \int_0^{2\pi} \frac{\cos^2\varphi, \sin^2\varphi}{K(\varphi)} \times \frac{d\varphi}{[1-\exp\{[-2\pi H_c(\varphi)/H](i+1/\omega\tau)\}]}\right]^{-\frac{1}{3}} e^{i\pi/3}, \quad (3)$$

where

$$H_c(\varphi) = \omega m^*(\varphi) c/e.$$

The nomenclature is the same as in Eq. (2). The relation between $k_H$ and $\varphi$ is shown in Fig. 5. In the free-electron

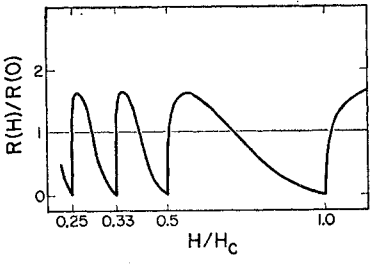


FIG. 6. Calculated absorption curve for infinite relaxation time.

case $\cos\varphi = k_H/k_F$, $\tau(\varphi)$ and $k(\varphi)$ are constant, and $m^*(\varphi) = m_e$, so that Eq. (3) reduces to

$$Z(H) \propto Z(0)\{1-\exp[(-2\pi i H_c/H)(1-i/\omega\tau)]\}^{\frac{1}{3}}, \quad (4)$$

where $Z(0)$ is the corresponding anomalous skin effect result given by Eq. (2).

A plot of the real part of the surface impedance normalized to its zero-field value for the case of a free electron gas and infinite relaxation time is shown in Fig. 6. The resonance minima $R(H)/R(0)=0$ occur exactly at the cyclotron fields, so that $m^* = eH_c/\omega c = e/\Delta(1/H)\omega c$. There is no attenuation in the size of the resonance signal with increasing harmonic number.

The effect of a finite relaxation time for a free electron gas is illustrated by the theoretical curves shown in Fig. 7. The cusp structure of the resonance minima is rounded off, the minima occur below the cyclotron fields, and the size of the resonance signals decreases with increasing harmonic number as fewer and fewer electrons complete orbits before suffering a collision. For $\omega\tau = 5$ the fundamental resonance occurs at $H = 0.90H_c$, while $\Delta(1/H) = 1/0.999H_c$; thus the periodicity of the resonance is a much better measure of the cyclotron

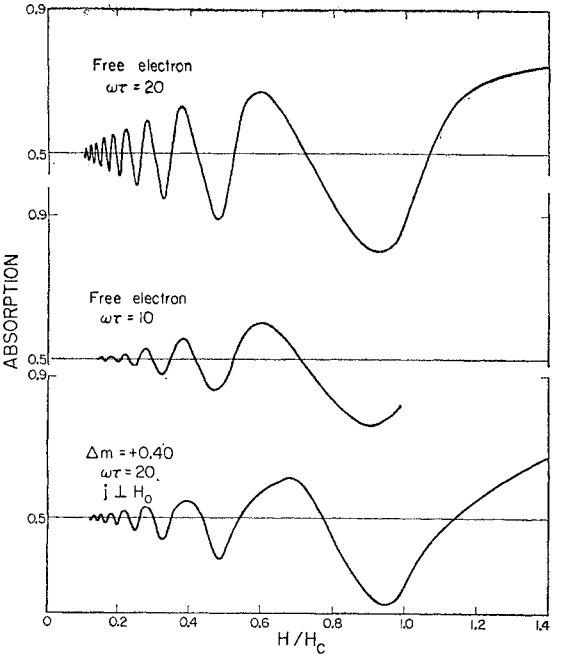


FIG. 7. Calculated absorption curves for finite relaxation times as indicated.

effective mass than the resonance fields themselves. A plot of reciprocal resonance fields against the harmonic number $n$ is shown in Fig. 8. This plot would be a straight line passing through the origin having slope one in the case of an infinite relaxation time. The displacement of the resonance fields is seen to be a constant in $1/H$; we shall call this displacement, normalized to $\Delta(1/H)$, the *phase shift* $\Delta\varphi$. In this case, $\Delta\varphi = +0.12$, and is a consequence of the finite relaxation time. This phase shift might be called "normal" or "expected," since it can be predicted if $\omega\tau$ is known. This is to be distinguished from the larger "anomalous" phase shifts which are sometimes experimentally observed.

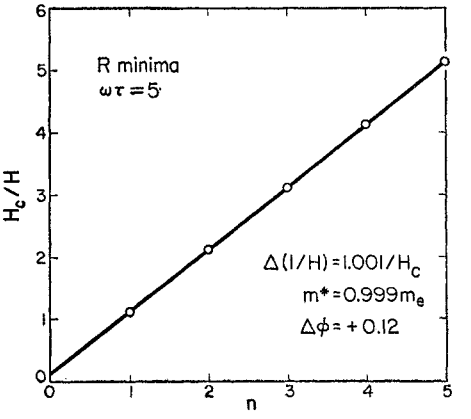


FIG. 8. Plot of reciprocal absorption minima fields against subharmonic number from a free-electron calculation with $\omega\tau = 5$.

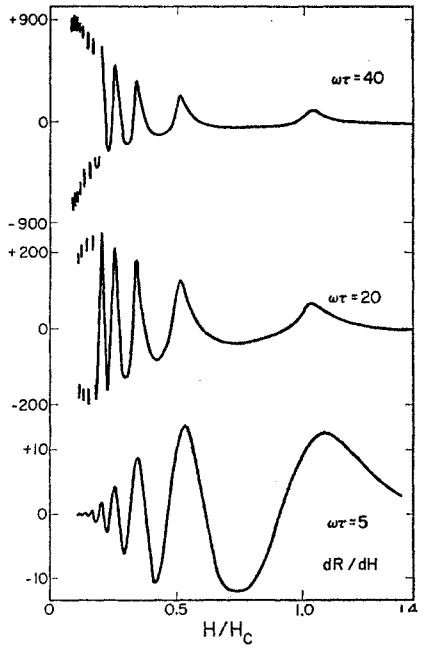


FIG. 9. Calculated absorption derivative curves for finite relaxation times as indicated. Ordinate in arbitrary units.

Absorption derivative curves for various $\omega\tau$ are shown in Fig. 9. For an infinite relaxation time, it can be seen from Fig. 6 that the derivative maxima occur at exactly the cyclotron fields. In the case of a finite relaxation time, these derivative maxima move to higher fields, but remain closer to the cyclotron fields than do the corresponding absorption minima. For $\omega\tau=5$, using absorption derivative maxima as the resonance criteria, $H/H_c=1.06$ at the fundamental resonance and $\Delta(1/H)=1/1.005H_c$ with $\Delta\varphi=-0.09$.

Thus for a free electron gas and $\omega\tau>5$, the mass values as derived from $\Delta(1/H)$ using either absorption minima or derivative maxima as the resonance criteria are in error by no more than 0.5% while use of the fundamental resonance alone may lead to errors as large as 10%. These conclusions are not changed radically in the presence of mass spread, which we discuss below.

One interesting feature of the derivative curves should be noted. As $\omega\tau$ is increased, the signal increases much more rapidly than in the corresponding absorption cases and the maximum signal occurs at higher and higher subharmonics. One consequence is that as $\omega$ is increased it is not necessary to scale magnetic field capabilities accordingly; thus at a low frequency $\omega_0$ it may be necessary to work with the fundamental and first few subharmonics, while at $N\omega_0$ it may be possible to use the $N$, $N+1$, . . . subharmonics, and the magnetic field requirements remain the same. However, we shall see that for some purposes it is desirable to examine the structure of the fundamental and first few subharmonics.

Table I gives the harmonic order and relative maximum signal size of the derivative curves for various $\omega\tau$. Fairly precise estimates of $\omega\tau$ may be made from the envelope of the absorption derivative curves.

We have made fairly extensive calculations, using an IBM 704 computer, of the resonance behavior as given by Eq. (3) in the case of mass spread and field tipping for $\mathbf{j}_{rf}$ both parallel and perpendicular to the static magnetic field. The computer was programmed so that the functions $K(\varphi)$, $m^*(\varphi)$, and $\tau(\varphi)$ could be independently compiled without rewriting the main program.

In all the calculations performed to date, $K(\varphi)$ has been constant; that is, the shape of the Fermi surface has been spherical, and $k_H/k_F=\cos\varphi$.

The mass function used has had the form

$$m^*(\varphi)=m_e\pm\Delta m(\cos\varphi)^2.$$

This is the lowest-order approximation which can be made; $m^*(\varphi)$ is extremal at $\varphi=\pm\pi$ ($k_H=0$) by symmetry and hence must be an even function about these points. Higher-order terms could easily be included.

Field tipping has been incorporated by means of the relaxation function $\tau(\varphi)$ in the following manner: $\omega\tau(\varphi)/2\pi$ is just the average number of revolutions an electron completes at the fundamental resonance, or the number of times it enters the skin depth in synchronism with the rf fields. If the magnetic field is parallel to the surface, $\omega\tau_0$ should be used, where $\tau_0$ is just the electron collision time, which we assume to be isotropic. However, when the field is tipped at an angle $\alpha$ with respect to the surface, an electron orbit $k_H$ will complete only $[\delta/\sin\alpha]/[2\pi v_D(k_H)/\omega]$ revolutions before spiraling out of the skin depth or into the surface. In this case, $v_D(k_H)=(k_H/k_F)v_F=v_F\cos\varphi$, and

$$\omega\tau(\varphi)=\min[\omega\tau_0 K/\cos\varphi\sin\alpha].$$

This rather elementary treatment ignores the statistics of orbit survival and, more importantly, the space and phase variations of the rf fields in the skin depth, but should give the correct dependence on $\alpha$ and $\varphi$. The constant $K\propto\delta\omega/2\pi v_F$ can be adjusted to compensate for the shortcomings of the model.

The integrand of Eq. (3) will be a very strong function of $\varphi$, especially at low fields if $\Delta m$ is large. A given

TABLE I. Subharmonic number and relative size of largest $dR/dH$ signals for free electrons.

| $\omega\tau$ | $n_{max}$ | Relative signal size |
|---|---|---|
| 1 | 1 | 0.3 |
| 2 | 1 | 2.3 |
| 3 | 1 | 5.5 |
| 5 | 2 | 14.0 |
| 10 | 3 | 59.3 |
| 20 | 6 | 236 |
| 30 | 9 | 534 |
| 40 | 11 | 950 |
| 50 | >12 | >1500 |
| 75 | >12 | >2700 |
| 100 | >12 | >3800 |

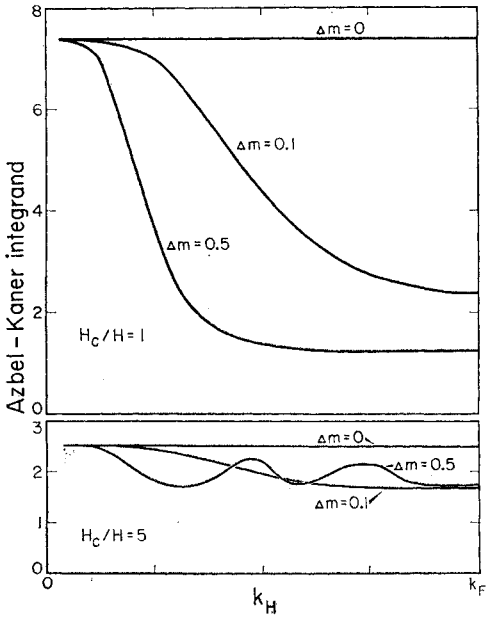


FIG. 10. The real part of the integrand of Eq. (3) for various values of the mass spread parameter at $H_c/H=1$ and $H_c/H=5$.

field corresponding to, say, the $N$th subharmonic of the central $k_H=0$ mass, may also correspond to the $N\pm1$ subharmonic at $k_H=\Delta k_H$, and also to the $N\pm2$ subharmonic at $k_H=\sqrt{2}\Delta k_H$, etc.; the number of nodes in the integrand is approximately $N(\Delta m/m_c)$. Thus the numerical integration of Eq. (3) becomes more and more difficult as $N$ and $\Delta m$ are increased. Figure 10 shows the behavior of the real part of the integrand at the fundamental and fifth subharmonic for $\omega\tau_0=20$ for several values of $\Delta m$; the polarization factor $\sin^2\varphi$, $\cos^2\varphi$ has been omitted in these curves only.

An instructive nomographic equivalent of these calculations can be given with the aid of Fig. 11. The spiral is the resonance factor

$$F=\{1-\exp[-(2\pi iH_c/H)(1-i/\omega\tau)]\}^{-1},$$

for $\omega\tau=20$. In the free electron case $Z(H)\propto Z(0)F^{-\frac{1}{3}}$; the constant of proportionality is such that at the convergence point of the spiral $Z(H)=Z(0)$, the anomalous skin effect results. In the arbitrary case there is a spread of $H_c/H$ at a given field because of mass spread, and the integration process is equivalent to the vectorial addition of such resonance factors over a range of $H_c/H$, suitably weighted by the appropriate polarization factor $\sin^2\varphi$ or $\cos^2\varphi$ and the geometry factor $K(\varphi)$. If the field is tipped, spirals for various $\omega\tau_0$ would be used, as explained above. The scale factor would again be chosen so that the limiting value at small fields is $Z(0)$. Pippard[23] has suggested a similar treatment.

One of the primary purposes for undertaking these calculations was an attempt to reproduce anomalously large phase shifts (of the order of $\Delta\varphi=+0.3$) observed experimentally in absorption derivative data. No phase shifts greater than $\Delta\varphi=\pm0.10$ were found for $\Delta m\leqq0.40$ using the $\Delta(1/H)$ of absorption derivative maxima as the resonance criteria, although somewhat larger phase shifts did occur using absorption minima.

As expected, the effect of mass spread and tipping was much less for perpendicular than for parallel polarization. The deviation of the mass values from the extremal value as derived from $\Delta(1/H)$ were typically of the order of $\Delta m/10$ for perpendicular polarization and $\Delta m$ for parallel polarization. Enhancement of the resonance signal in the cases of large $\Delta m$ by field tipping was verified.

The effect of mass spread, polarization, and field tipping on the *shape* of the absorption resonance curves is also of some interest. To a first approximation, the effect of mass spread is an apparent decrease in $\omega\tau$, as was first suggested by Phillips.[32] In addition, the absorption minima are narrowed for positive $\Delta m$ with perpendicular polarization or negative $\Delta m$ with parallel polarization, and are broadened in the converse cases. These effects are shown in Fig. 7 where for $\omega\tau_0=20$, $\Delta m=+0.20$, and perpendicular polarization, the resonance is more characteristic of a free-electron resonance with $\omega\tau_0=10$, and the absorption minima are narrowed. This curve is very similar to the data of Galt[16] in zinc, using circular polarization.

Absorption derivative curves are much more sensitive to changes in line shape, and it is difficult to make any general qualitative comments about them. Two interesting features should be mentioned, however. Extra structure often appears in the fundamental and low harmonics, which for large mass spread sometimes forms extra peaks, or "satellite" lines; in addition the envelope of the high harmonics can become nonmonotonic. These effects have been observed experimentally and may

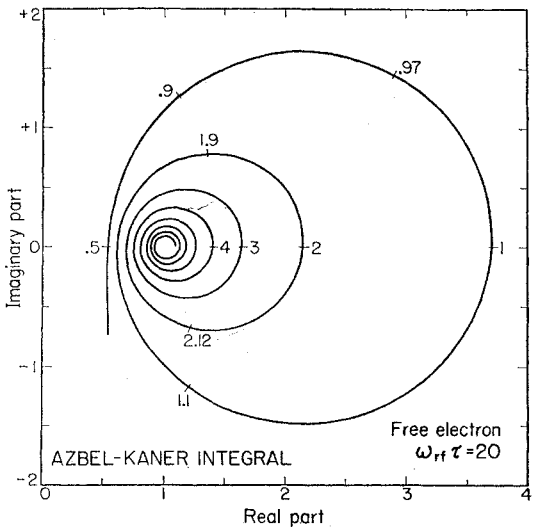


FIG. 11. The resonance factor $F$ for free electrons with $\omega\tau=20$. The parameter along the spiral is $H_c/H$.

[32] J. C. Phillips, Phys. Rev. Letters **3**, 327 (1959).

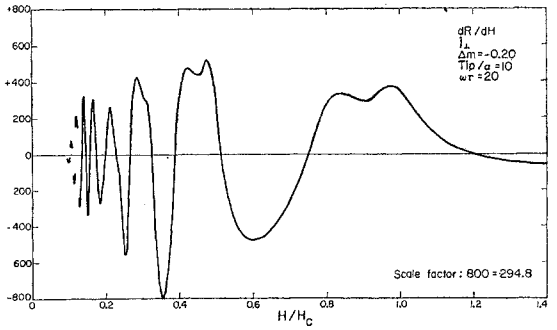


FIG. 12. Calculated absorption derivative curve for $\Delta m=-0.20$, $K/\sin\alpha=10$, and $\omega\tau_0=20$ with $\mathbf{j}_{rf}$ perpendicular to $\mathbf{H}$.

serve to distinguish between mass spread and relaxation time anisotropy. A typical example is shown in Fig. 12; the scale factor is such that the maximum signal (at the second harmonic derivative minima) is 294.8/800 of the maximum signal in the free-electron case with the same $\omega\tau_0$.

Calculations were also made for the case in which two independent groups of carriers were present with various mass and population ratios by summing free-electron resonance factors. The case of mass ratio 2:1 is of particular interest for the work in copper. Some results of these calculations are shown in Fig. 13.

A limited number of complete copies of these calculations and the computer programs used are available from the authors on request.

## III. EXPERIMENTAL ASPECTS

The measurements reported in this paper were made at 24 kMc/sec using a standard microwave reflection spectrometer[1] similar to those widely used in electron spin resonance experiments. The sample formed one wall of a resonant cavity at helium temperature, and the spectrometer was balanced so that $\Delta Q/Q=\Delta R/R$, where $R$ is the real part of the sample surface impedance. We confine our discussion here to three main topics: (A) samples, (B) cavity design and sample mounting techniques, and (C) signal detection methods.

### A. Samples

The success of the work reported in this paper is in large measure due to the high quality of the copper sample used, which was kindly provided by Dr. J. E. Kunzler of the Bell Telephone Laboratories. Some concept of the excellence of this sample can be gained by considering residual resistivity ratios $S=(\rho_{300°K}/\rho_{4°K})$. For ordinary commercial copper, $S$ is about 50, and zone-refined copper available before 1959 yielded values of $S\leq 1000$; Langenberg[33] reported that some natural samples, notably from the Lake Superior region, have unusually high ratios, 8600 being the maximum value found. However, this material is not very suitable for cyclotron resonance experiments, since it is usually polycrystalline, nonhomogeneous, and has rock inclusions. The Bell Telephone Laboratory sample used in the present work was a large single crystal about 3 cm in diameter and 5 mm thick; its residual resistivity ratio was between 5000 and 10 000.

Specimens having this high degree of purity and crystalline perfection may be easily damaged if they are shaped mechanically, and thus must be cut chemically. In this case, a (110) surface was cut with concentrated nitric acid using a continuous-string acid saw. The resulting surface was then smoothed with acid-saturated felt, and finally electropolished with a 50-50 phosphoric acid-water solution.

### B. Cavity Design and Sample Mounting Techniques

A systematic investigation of cyclotron resonance requires the following degrees of freedom: (i) orientation of the static magnetic field with respect to the crystal axes in the plane of the sample surface, (ii) small-angle tipping of the magnetic field with respect to the sample surface, and (iii) the direction of linear rf currents with respect to the magnetic field (rf polarization).

The first of these was accomplished by mounting the sample in the horizontal plane and rotating the whole magnet about a vertical axis. Relative angles of the magnetic field axis could be easily set with a precision of $\frac{1}{8}$ degree.

Field tipping was accomplished by raising the magnet and inserting calibrated blocks under one end; the maximum tipping which could be achieved in this manner was 3°.

The ideal way to assure linear polarization would be to use a rectangular cavity. However, this would require

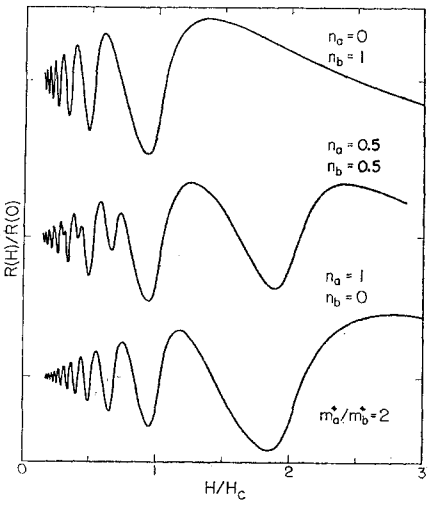


FIG. 13. Calculated absorption curve for two independent free electron groups with mass ratio 2:1; relative number of electrons as indicated.

[33] D. N. Langenberg, Doctoral dissertation, University of California, Berkeley, California, 1959 (unpublished).

remounting the sample to change the direction of polarization with respect to the crystal axes. The present experiments were performed using a cylindrical $TE_{111}$ cavity with the sample forming the bottom wall. The current lines across an end wall of this mode are not strictly linear, but are slightly divergent. A crude estimate indicates that 85% of the current density lies within $\pm 10°$ of a symmetry axis through the center of the end wall; this is a satisfactory situation since changes of 10° in the polarization direction do not appreciably affect the resonances.

This mode is degenerate in the ideal case and may be split into two orthogonal modes by a slight ellipticity or side-wall perturbation. This has been accomplished in the present case with a phosphor-bronze "mode-splitting pin" attached to the top coupling wall; the pin is close and parallel to the side wall; but does not actually touch it. The whole coupling wall may be rotated with respect to the cavity body and attached sample, so that the end-wall symmetry axes of the two orthogonal modes may be set along any desired crystal axis in the sample surface. At any position of the pin, data may be taken near two orthogonal crystal axes with $\mathbf{j}_{rf}$ either parallel or perpendicular to the axes by simply shifting the klystron frequency from one mode to another and rotating the magnet 90°. The mode splitting was about 100 Mc/sec or 50 cavity half-widths at helium temperature.

The whole cavity (sample, body, and coupling wall together) could be rotated on the wave guide, thus adjusting the degree of coupling to either mode, which is proportional to the sine of the angle between the fields in the guide and cavity.

Magnetic field, crystal axis, and polarization orientation was accomplished in the following manner: Electron paramagnetic resonance signals vanish when rf currents are perpendicular to the applied magnetic field, so that the mode-splitting pin could be located by rotating the magnet to minimize the signal from a small piece of organic free radical permanently mounted at the center of the sample; the closest crystal symmetry axis (⟨100⟩ or ⟨110⟩) was then located by the symmetry of the cyclotron resonance data. Both of these procedures could be accomplished with a maximum absolute error of $\frac{1}{2}°$.

The cavity side wall was made of a thin shell of electrodeposited copper having a residual resistivity ratio of about 750, so that the microwave losses in this portion of the cavity were only about $\frac{1}{10}$ of what they would have been had ordinary commercial copper been used. One undesired consequence of this high-conductivity material was an attenuation and field-dependent phase shift in the modulation field. This last difficulty was largely overcome by electrodepositing only the first few microns (or skin depths) with high-purity copper; the conductivity of the rest of the cavity body was made low by adding sodium-arsenate to the electrodepositing solution.

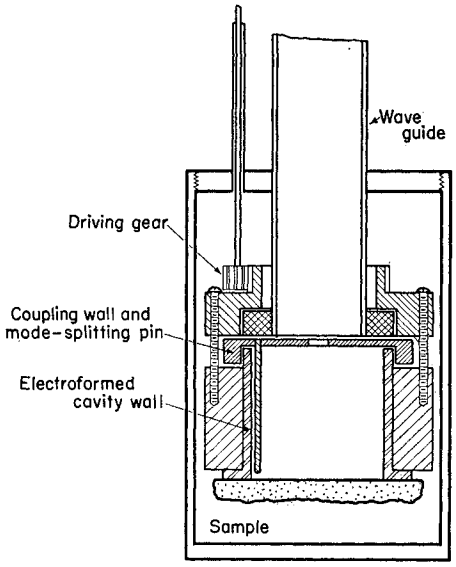


FIG. 14. Schematic cutaway view of the cavity and sample assembly.

During the early part of this work the sample was lightly clamped onto the cavity body using phosphor-bronze springs in order to avoid possible damage to the sample from differential thermal contraction which might occur if the sample were soldered. This arrangement gave unsteady contacts between sample and cavity and gave a variable cavity $Q$. Later, the sample was soldered to the cavity body with indium, which remains plastic at 4°. Since that time, the sample has been cooled approximately 50 times with no apparent damage.

The whole sample-cavity assembly was enclosed in a helium-tight copper can sealed with glycerine and Ivory soap. The can contained a helium exchange gas. Thus it was not necessary to pump below the λ point to prevent noise from helium bubbling in the cavity, and the thermal stability was excellent.

The sample-cavity assembly is illustrated in Fig. 14.

### C. Signal Detection Methods

Either dc (homodyne) or ac (field-modulated) signal detection methods could be used in the present experiments. In the first case, the signal is proportional to $R(H)$, and in the second case to $dR/dH$. For low $\omega\tau$, the absorption signal is appreciable only for low-order subharmonics and the lines are therefore very broad (of the order of $H_c/2n$, where $n$ is the subharmonic number). Because of the high conductivity of the sample and cavity, it is difficult to modulate an appreciable fraction of a linewidth, especially at audio frequencies. Under these circumstances dc detection may be more sensitive, but always has the disadvantage that crystal noise is large and drift problems may arise. If the field is modulated, crystal noise is reduced by a factor proportional

to $1/f$, and a phase-sensitive detector may be used, whose effective bandwidth may be reduced by integration ($\Delta f \sim 1/RC$). One difficulty with high-frequency ac detection is the occurrence of microphonic effects caused by the modulation field; these often take the form of reproducible mechanical resonances and cavity "squeezing" due to eddy currents.

Both methods of detection have been used in the present work and are about equivalent except for one factor. The rf magnetoresistance of copper between zero field and $H_c$ is a monotonic function having a total amplitude approximately ten times the maximum cyclotron resonance absorption signal. Thus, if dc detection is used, the cyclotron resonance signal appears only as a fairly minor perturbation; on the other hand, if ac detection is used, the magnetoresistance appears only as a nearly constant bias signal in the resonance region, since its derivative is a relatively weak function of field. This is shown as the dashed line in Fig. 1. All data presented in this paper were taken using field modulation.

The modulation frequency used in this work was $7\frac{1}{2}$ cps; this choice was dictated partially by the availability of existing equipment. Even at this relatively low frequency, the modulation amplitude at the surface of the sample at helium temperatures is only 5% of the applied modulation because of eddy current losses in the cavity walls and sample.

The $7\frac{1}{2}$-cps frequency was generated by digital frequency division from the 60-cps line; since an exact even harmonic was used, any 60-cps pickup in the detection system was integrated to zero by the phase-sensitive detector, and shielding problems were held to a minimum. The $7\frac{1}{2}$-cps signal was then applied to two parallel relay-driving circuits, one of which could be delayed (phase shifted) up to one-half cycle with respect to the other. Two mercury-wetted relays (Clare HG 1003) were used, one for field modulation and the other for signal demodulation. The $7\frac{1}{2}$-cycle resonance signal was amplified using a Liston-Becker dc chopper amplifier with its chopper motor disconnected; this instrument has a nominal center frequency of 8 cps and a 2-cps bandwidth.

Figure 15 is a schematic drawing of the ac detection described above.

## IV. EXPERIMENTAL RESULTS AND INTERPRETATION

The Pippard model[28] of the Fermi surface of copper is shown in Fig. 16. It may be described fairly accurately as a sphere with "necks" in the ⟨111⟩ directions which contact the zone boundaries. These "necks" have almost circular cross sections at the zone boundaries and subtend an angle of about 17° from the center of the zone. The more recent de Haas-van Alphen[34] and ultrasonic resonance[35] experiments have confirmed these features.

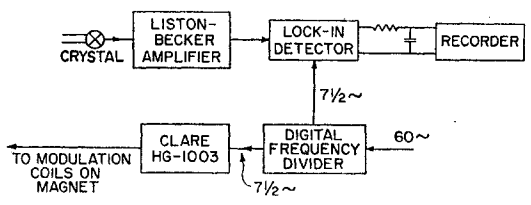


FIG. 15. Block diagram of the ac detection apparatus.

All the data presented in this paper were taken with the static magnetic field in a (110) plane. Since this plane has twofold and reflection symmetry, only one quadrant need be considered. We shall specify the direction of the magnetic field in the plane with respect to the ⟨100⟩ axis by $\theta$; the ⟨111⟩ direction is at $\theta = 55°$ and the ⟨110⟩ at $\theta = 90°$.

Figure 17 shows the (110) plane through the center of the Fermi surface in the extended zone scheme; the small ellipses represent the out-of-plane contact areas. The shaded segments represent the angular regions in which various classes of stationary orbits exist.

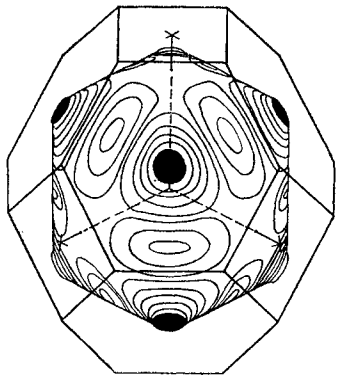

FIG. 16. The Pippard model (1957) for the Fermi surface of copper derived from anomalous skin effect measurements.

These stationary orbits may be divided into four main classes as follows: (i) "belly" orbits, (ii) "mass two" orbits, (iii) "negative mass" orbits, and (iv) "neck" orbits.

Belly orbits, labeled $A$ and $E$ in Fig. 17, encircle the spherical part of the Fermi surface and are closed in a single zone. The plane of these orbits in $\mathbf{k}$ space passes through the center of the Brillouin zone $\Gamma$ ($k_H = 0$). These are the only stationary orbits in the case of a free electron sphere; in copper, because of the zone contacts, belly orbits do not exist over the full 90 degrees of field orientation and other types of stationary orbits do exist.

The "mass two" orbits, labeled $B$, $C$, and $D$, are closed in two zones, or, alternatively, undergo two Bragg reflections at zone boundaries. The plane of these orbits passes through the symmetry point $L$ at the center of a hexagonal face, which is also the center of the contact area; a simple consideration of neighboring parallel orbits shows that these orbits are indeed stationary. These orbits are essentially two belly orbits joined across the narrow neck and hence "dumbbell" shaped;

[34] D. Shoenberg, Phil. Mag. 5, 105 (1960).
[35] R. W. Morse, A. Meyers, and C. T. Walker, Phys. Rev. Letters 4, 605 (1960).

we can see from Eq. (2) that they have a cyclotron mass very close to twice the mass of a belly orbit.

The negative mass orbits $F$ and $H$-$H'$ are closed in four zones; that is, they undergo four Bragg reflections. They have "negative" masses because their cyclotron rotation is in the opposite sense from that of a free electron. The cross section of an $F$ orbit, appropriately referred to as the "dog's bone" by Shoenberg,[34] is also shown in Fig. 17; we can see that as the energy is increased the area of the orbit decreases, so that Eq. (1) yields a negative mass. The orbits $H$-$H'$ have also been observed in the de Haas-van Alphen effect and have been termed the "four-cornered rosettes" by Shoenberg.

Neck orbits, labeled $G$ (not shaded), are a special case of mass two orbits. We do not expect them to have masses twice the belly mass, however. The orbit in the plane of the zone boundary will have a relatively small cross-sectional area, which will rapidly increase as the

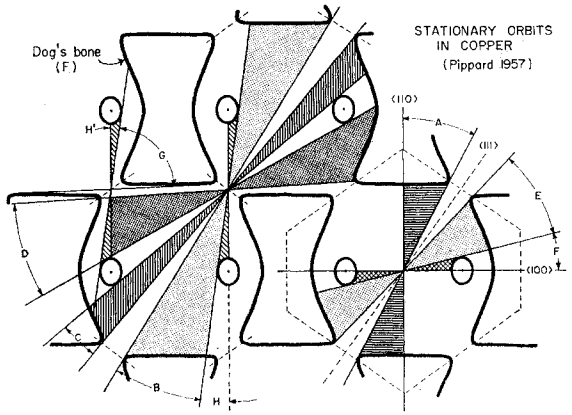


FIG. 17. Projection of the Fermi surface of copper onto the (110) plane in the extended zone scheme. The shaded areas represent angular regions of the various classes of stationary orbits discussed in the text. Magnetic field directions are normal to the orbit planes.

plane of the orbit (e.g., the magnetic field) is rotated in either direction; the mass values therefore should be highly anisotropic.

These are certainly not the only stationary orbits which exist in copper. At $\Gamma$ there are extended orbits closed in 3, 5, . . . , $2n+1$, . . . zones which might be called "mass $2n+1$" orbits in analogy to "mass two" orbits, and at $L$ there are orbits closed in 4, 6, . . . , $2n$, . . . zones, or "mass $2n$" orbits. These orbits exist in small angular regions to either side of a ⟨111⟩ direction; the larger $n$, the smaller the region. In addition, there are various types of "open" orbits, that is, orbits which never close. A trivial example is the limit $n=\infty$; the orbit in this case is along the ⟨111⟩ direction in $\mathbf{k}$ space. Various types of open orbits and the regions in which they occur have been described in some detail by Lifshitz and Peschanskii[21] but need not concern us further here. Direct observation of open orbits in copper in magnetoresistance saturation has been reported by

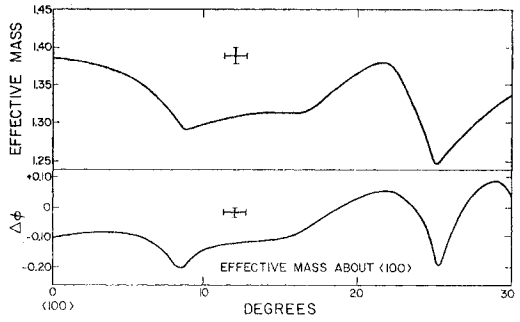


FIG. 18. Mass and phase shift anisotropy of the belly orbits $A$.

Alekseevski and Gaidukov[36] and by Klauder and Kunzler.[37] Cyclotron resonance data have been taken for all values of $\theta$ from 0° to 90°, with rf polarization essentially perpendicular and parallel to the static magnetic field. The $\theta$ increments were small enough to follow the mass anisotropy and in some cases were only $\frac{1}{2}$°. Field tipping was used wherever necessary to identify harmonic series corresponding to different groups of carriers.

Recorder tracings were made for both increasing and decreasing fields so that time-constant delays in the phase-sensitive detector could be averaged out. The cyclotron fields corresponding to derivative maxima were then punched on IBM cards and the periodicity $\Delta(1/H)$ and phase shifts $\Delta\varphi$ computed by a least-squares method. The rms errors in the masses and phase shifts were typically 0.5%.

The most useful data were obtained with perpendicular polarization, and all results discussed below were taken using this mode unless otherwise stated. In general, traces taken with parallel polarization were one or two orders of magnitude smaller in signal amplitude, highly anisotropic, and very tip dependent. Interpretation of these data was often impossible because two or more groups of carriers were present and "satellite" lines were relatively strong and confusing.

We start our specific consideration of the data at $\theta=0°$, that is, with the static magnetic field along the ⟨100⟩ direction. Here the belly orbits $A$ are present over a wide range of $k_H$, and the resonance signal has the largest amplitude observed, about 1% of $Z(0)$. The negative mass orbits $H$-$H'$ also exist here, but are not observed, probably because any resonance signal from them is dwarfed by the strong belly resonance. The recorder tracing shown in Fig. 1 was taken here; $m^*=1.39$ and $\Delta\varphi=-0.09$.

The anisotropy of the mass and phase shift of the $A$ belly orbits is shown in Fig. 18. These data were symmetric about $\theta=0°$ within experimental error. One feature of these curves which should be noted is the remarkable correlation between $m^*$ and $\Delta\varphi$. This

[36] N. E. Alekseevskii and Yu. P. Gaidukov, Soviet Phys.—JETP **10**, 481 (1960).

[37] J. R. Klauder and J. E. Kunzler, Phys. Rev. Letters **6**, 179 (1961).

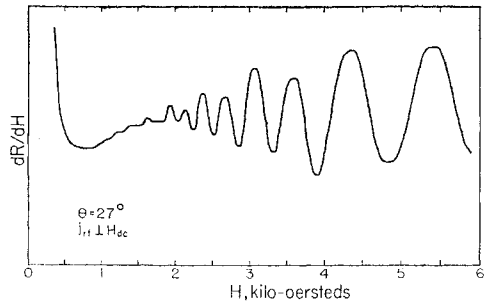


FIG. 19. Experimental absorption derivative trace at $\theta=27°$ with $\mathbf{j}_{rf}$ parallel to $\mathbf{H}$. Stationary orbits of both belly type $A$ and "mass two" type $B$ are present.

phenomenon is characteristic of all the data. Another feature is the dip at $\theta=8°$, the angle at which the $H$-$H'$ orbits cease to exist.

The magnitude of the signal from the $A$ orbits decreases with increasing $\theta$ because the range of $k_H$ over which such orbits exist decreases, becoming zero at $\theta=28°$.

The "mass two" $B$ orbits, which start at $\theta=8°$, are not observed until $\theta=14°$, probably for the same reason the $H$-$H'$ mass was not seen. A recorder tracing with signals from both the $A$ and $B$ orbits is shown in Fig. 19. The mass ratio is very nearly 2:1, so that every other harmonic of the $B$ mass is coincident with an $A$ harmonic. A reciprocal field plot of these data is shown in Fig. 20. The odd harmonics of the $B$ mass may be erroneously interpreted as belonging to a mass one-half the actual $B$ mass with $\Delta\varphi\approx\pm0.5$. That such is not the case is indicated by field-tipping data (see Fig. 23) and the excellent agreement of the "mass two" interpretation with the Pippard model.

To facilitate comparison of the ratio $m_A^*/m_B^*$, the $B$ orbit mass and phase shift is shown in Fig. 21 between 14° and 31° as derived from odd harmonics only. The actual mass is, of course, twice that indicated, and the phase shift very near zero. The heavy line between 0° and 30° represents the $A$ mass as in Fig. 18. Again we see a strong correlation between $m^*$ and $\Delta\varphi$. The peak at 25° corresponds closely to the angle at which the $A$ orbits are expected to vanish. It is impossible to determine where the $A$ signal actually fades out because the even-numbered $B$ harmonics are coincident with them; the $A$ mass shown beyond 25° is probably only the even $B$ harmonics. The $B$ mass disappears at 31° as expected.

The existence of $B$ orbits between 8° and 14° is strongly indicated by parallel polarization data. Figure 22 shows recorder traces taken at 11°; the mode-splitting pin was on the ⟨100⟩ axis so $\mathbf{j}_{rf}$ was 70° from the static magnetic field in the upper trace, in which there is only a single, strong signal from $A$ orbits, and 11° from the field direction in the lower trace, which shows two weak signals, presumably from $A$ and $B$ orbits. The anisotropy of the masses was not investigated in this mode.

The region between 31° and 46°, where belly orbits are prohibited by the contact areas, gave very complicated results. This is just the region where "mass $2n$" and "mass $2n+1$" orbits are expected over narrow angular ranges. No attempt was made to take systematic data in this region, but the behavior here was in qualitative agreement with the Pippard model.

At 46° the belly mass $E$ appears and can be followed to approximately 78°. The "mass two" orbits $D$ also come in around 64° and fade out at 80°; they are shown in Fig. 21 in the same manner as the $B$ orbits. The negative mass "dog's bone" orbits $F$ are seen from 78° to the ⟨110⟩ direction, $\theta=90°$.

The regions about 65° and 80°, where the $D$ orbits vanish, are extremely complicated; two and three masses are simultaneously present, and the signal strength is very weak. It was impossible to sort out the masses with any confidence in these regions. The break in the $E$ belly mass at 65° represents the best interpretation of the data in this region but is inconsistent with

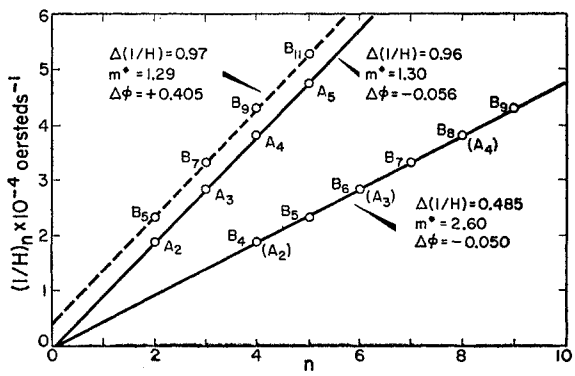


FIG. 20. Reciprocal field plot of the data in Fig. 19. The dotted line represents an erroneous interpretation of the $B$ subharmonic series, as explained in the text, using only the odd subharmonics.

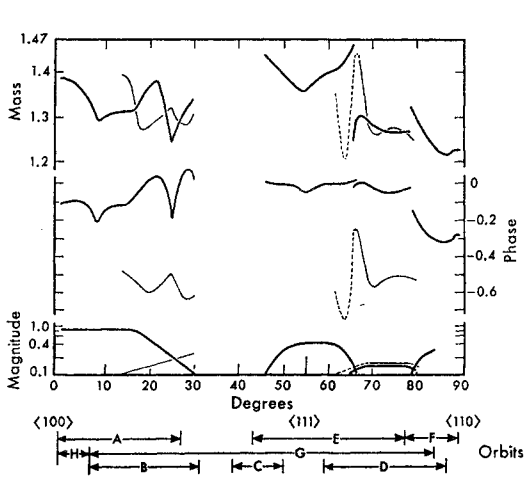


FIG. 21. Mass, phase shift, and relative signal amplitude anisotropy of stationary orbits in copper. The "mass two" orbits $B$ and $D$ have been recorded as derived from the odd subharmonics only, as shown in Fig. 20, and are indicated by the lightweight lines.

the Pippard model and is probably due to erroneous identification of "satellite" lines and perhaps resonances from neck orbits $G$ which do not appear often enough, if at all, to be positively identified.

An example of the use of field tipping to distinguish between resonances caused by different groups of carriers is shown in Fig. 23, taken at $\theta=75°$; the belly orbits $E$ and "mass two" orbits $D$ are both present, as indicated. The $D$ resonance is attenuated by tipping, while the $E$ resonance is enhanced, indicating that $E$ orbits do indeed have a large mass spread.

The dog's bone orbit $F$ is unique in that it is the only negative mass observed and gives anomalously large phase shifts, $\Delta\varphi\sim 0.3$. All the other phase shifts observed are very close to zero.

The effective mass of orbits around the smallest part of the neck (for $H_{dc}$ along a $\langle 111\rangle$ axis) is of particular interest. While the neck orbits $G$ are stationary, the range of $k_H$ for which the drift velocity is small and for which perpendicular polarization is the favorable mode is much less than the corresponding range of $k_H$ for belly orbits. Thus it is reasonable that the strong resonance signals from belly orbits obscure any signal from neck orbits. The belly resonance is suppressed, however, if parallel polarization is used and stationary neck orbits may be observed for $H_{dc}$ in a region between the $\langle 110\rangle$ and the $\langle 111\rangle$ axes, where the gradient of the Fermi surface, $\Delta_k E(\mathbf{k})$, in the effective zone has a large component parallel to the field. Orbits in the plane of the zone boundary cannot be observed since this resonance is also suppressed by parallel polarization. No resonances which could be identified as neck orbits were observed with $H_{dc}$ to the other side of the $\langle 111\rangle$, perhaps because the plane of the neck orbits in this region is nearly tangent to the Fermi surface and hence

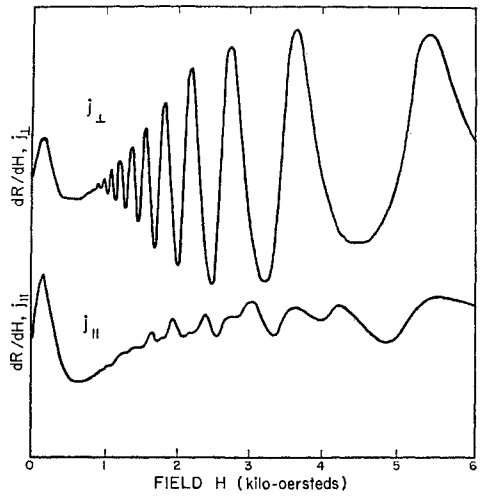


FIG. 22. Experimental absorption derivative traces at $\theta=11°$ with $\mathbf{j}_{rf}$ along the $\langle 110\rangle$ axis 79° from $\mathbf{H}$ (top panel) and along the $\langle 100\rangle$ axis 11° from $\mathbf{H}$ (bottom panel). Belly orbits $A$ dominate the signal in the top panel; both the belly orbits $A$ and the "mass two" orbits $B$ may be seen in the bottom panel.

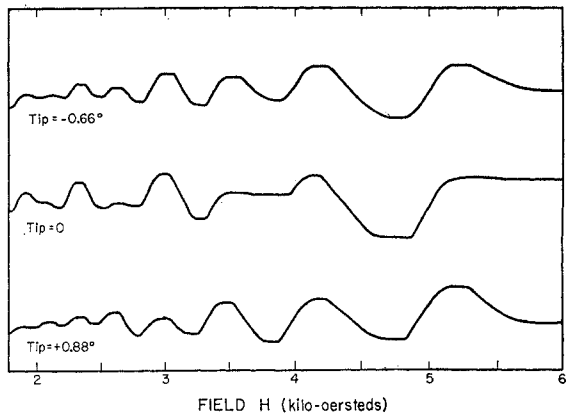


FIG. 23. Experimental absorption derivative traces at $\theta=75°$ for various angles of field tipping as indicated; $\mathbf{j}_{rf}$ along the $\langle 100\rangle$ axis 15° from $\mathbf{H}$. Belly orbits $E$ and "mass two" orbits $D$ are both present, as verified by the different effects of field tipping.

the cyclotron mass very large. A plot of these data is shown in Fig. 24; the mass increases rapidly as $\theta$ approaches 90°, since the area of the orbits in momentum space rapidly increases. An effective mass of 0.6 $m_e$ may be assigned to orbits around the smallest part of the neck by extrapolation.

Ziman[31] has suggested that the relaxation time of neck orbits parallel to the zone face should be significantly less than that of belly orbits. Because of an inability to distinguish between mass spread and true relaxation time effects, only a lower limit of one-half the belly $\omega\tau$ can be placed on the relaxation time of the neck orbits described above. A higher $\omega\tau$ (say at a higher microwave frequency) might allow these effects to be separated to a greater degree, so that relaxation time anisotropy could be investigated in general.

Determination of the temperature dependence of the cyclotron resonance signals might also yield some information about collision processes. Fragmentary data at 2°K show no detectable differences from data taken at 4.2°K, indicating that the relaxation time is indeed impurity and defect limited.

We would like to take this opportunity to point out that the discrepancies between the mass values reported

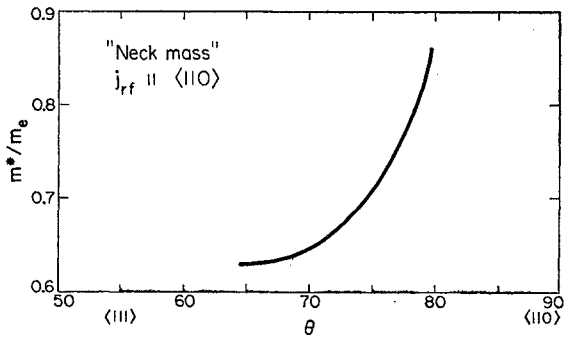


FIG. 24. Mass anisotropy of neck orbits $G$; $\mathbf{j}_{rf}$ along the $\langle 110\rangle$ axis.

in this paper and in our earlier work,[20] which in some cases are as large as 8%, are due to the arbitrary rf polarization used in the preliminary experiments.

Some mention should be made of the structure below 500 oe, which can be seen in all the experimental resonance curves. This "zero-field" effect was originally observed by Kip *et al.*[9] in tin using ac detection, and was thought to be due to microphonic effects caused by the modulation field. Similar structure has now also been seen in aluminum[15] as well as copper using both dc and ac detection methods and appears to be characteristic of high-purity, single-crystal samples. The effect occurs at fields where orbits are not being completed but in which the curvature of the trajectories is important, so that neither high- nor low-field approximations can be made. Therefore no theoretical explanation is available as yet. The effect appears to be very isotropic, so it is unlikely that any detailed information can be derived from it. More recently Khaikin[38] has reported the observation of fine structure in the surface impedance of tin below 10 oes.

## V. CONCLUSIONS

With the exception of the unexplained phase shifts and the absorption at low magnetic fields, the results obtained from cyclotron resonance experiments in copper are consistent with the known Fermi surface geometry and with the theory of Azbel' and Kaner. Stationary orbits, that is, orbits with extremal effective mass and zero drift velocity, dominate the resonances. An infinite number of classes of stationary orbits exist in copper because the Fermi surface contacts the zone boundaries. The effective mass and phase shifts of several classes of stationary orbits have been determined as a function of the orientation of the static magnetic field in a (110) surface.

Pippard[23] has suggested that the phase shifts and their correlation with mass values may be caused by mass spread; exact calculations, however, show that while such phase shifts are present in absorption minima, they do not occur in absorption derivative maxima.

An alternative explanation is that phase shifts are due to many-body or orbit interaction effects. Consider the dog's bone orbits $F$, which give the largest phase shifts; this is the only negative mass observed, and there is a large population of nonstationary belly orbits present which are not observed but which may interact with the stationary dog's bone orbits in such a way as to impress a phase shift. The presence of "kinks" at $\theta=8°$, where the unobserved negative mass orbits $H$-$H'$ vanish, and at $\theta=55°$, where the unobserved neck orbit is parallel to the zone boundary, is further evidence that such mechanism may be present.

Experiments to determine the temperature and frequency dependence of cyclotron resonance signals might yield information about collision processes and relaxation time anisotropy; such work should probably be done at higher microwave frequencies for optimum results.

## ACKNOWLEDGMENTS

We would like to thank Dr. J. E. Kunzler of the Bell Telephone Laboratories for supplying the copper sample used in this work, and gratefully acknowledge many discussions with Dr. J. C. Phillips, Dr. J. M. Ziman, and Dr. Walter Harrison.

[38] M. S. Khaikin, Soviet Phys.—JETP **12**, 152 (1961).